



# Characterizing the gradients of structural covariance in the human hippocampus

Shahrzad Kharabian Masouleh<sup>a,b,\*</sup>, Anna Plachti<sup>a,b</sup>, Felix Hoffstaedter<sup>a,b</sup>, Simon Eickhoff<sup>a,b</sup>, Sarah Genon<sup>a,b</sup>

<sup>a</sup> Institute of Neuroscience and Medicine (INM-7: Brain and Behaviour), Research Centre Jülich, Jülich, Germany

<sup>b</sup> Institute of Systems Neuroscience, Heinrich Heine University Düsseldorf, Düsseldorf, Germany

## ABSTRACT

The hippocampus is a plastic brain structure that has been associated with a range of behavioral aspects but also shows vulnerability to the most frequent neurocognitive diseases. Different aspects of its organization have been revealed by studies probing its different neurobiological properties. In particular, histological work has shown a pattern of differentiation along the proximal-distal dimension, while studies examining functional properties and large-scale functional integration have primarily highlighted a pattern of differentiation along the anterior-posterior dimension.

To better understand how these organizational dimensions underlie the pattern of structural covariance (SC) in the human hippocampus, we here applied a non-linear decomposition approach, disentangling the major modes of variation, to the pattern of gray matter volume correlation of hippocampus voxels with the rest of the brain in a sample of 377 healthy young adults. We additionally investigated the consistency of the derived gradients in an independent sample of life-span adults and also examined the relationships between these major modes of variations and the patterns derived from microstructure and functional connectivity mapping.

Our results showed that similar major modes of SC-variability are identified across the two independent datasets. The major dimension of variation found in SC runs along the hippocampal anterior-posterior axis and followed closely the principal dimension of functional differentiation, suggesting an influence of network level interaction in this major mode of morphological variability. The second main mode of variability in the SC showed a gradient along the dorsal-ventral axis, and was moderately related to variability in hippocampal microstructural properties.

Thus our results depicting relatively reliable patterns of SC-variability within the hippocampus show an interplay between the already known organizational principles on the pattern of variability in hippocampus' macrostructural properties. This study hence provides a first insight on the underlying organizational forces generating different co-plastic modes within the human hippocampus that may, in turn, help to better understand different vulnerability patterns of this crucial structure in different neurological and psychiatric diseases.

## 1. Introduction

The hippocampus is a complex, phylogenetically preserved brain structure, located within the medial temporal lobe. Characterizing its functional pattern, multiple studies have demonstrated its involvement in different domains of human behavior including memory functions (Bonnici et al., 2013; Eichenbaum, 2004; Maren and Holt, 2000; Stella and Treves, 2011), spatial navigation (Chersi and Burgess, 2015), emotion (Plachti et al., 2018; Strange et al., 2014) and creative thinking (Chersi and Burgess, 2015). The variety of tasks and behavioral domains that are associated with this phylogenetically old brain structure hence demonstrates its crucial role in the whole cognitive system.

Neurobiologically, hippocampus' direct and indirect connections to cortical and subcortical structures place it at the cross-road of information transfer between distinct brain regions and as an important

component of the brain's large scale networks (Clawson et al., 2019; Dalton et al., 2019; Mitra et al., 2016; Ward et al., 2014). Accordingly, hippocampal alterations are reported within the most frequent neurodegenerative and psychiatric diseases, such as Alzheimer's disease (Allen et al., 2007; Halliday, 2017), schizophrenia (Lieberman et al., 2018), depression (Fateh et al., 2019; Kemmotsu et al., 2013) and anxiety (Cha et al., 2016) disorders where changes in its functional and morphological properties are linked to symptom severity and progression of the disease.

Within healthy individuals, the hippocampus structure is known to be very plastic exhibiting one of the most unique phenomena of the adult mammalian brain, namely, the development of new neurons throughout the life span (i.e. neurogenesis). Presumably partially related to this unique property, at the macroscopic level, plastic changes within the hippocampus are documented based on in-vivo MRI measurements. For example, it has been shown that taxi drivers with expert navigation

\* Corresponding author. Institute of Neuroscience and Medicine (INM-7: Brain and Behaviour), Research Centre Jülich, Jülich, Germany.

E-mail addresses: [s.kharabian@fz-juelich.de](mailto:s.kharabian@fz-juelich.de) (S. Kharabian Masouleh), [a.plachti@fz-juelich.de](mailto:a.plachti@fz-juelich.de) (A. Plachti), [f.hoffstaedter@fz-juelich.de](mailto:f.hoffstaedter@fz-juelich.de) (F. Hoffstaedter), [s.eickhoff@fz-juelich.de](mailto:s.eickhoff@fz-juelich.de) (S. Eickhoff), [s.genon@fz-juelich.de](mailto:s.genon@fz-juelich.de) (S. Genon).

<https://doi.org/10.1016/j.neuroimage.2020.116972>

Received 20 January 2020; Received in revised form 29 April 2020; Accepted 17 May 2020

Available online 23 May 2020

1053-8119/© 2020 The Authors. Published by Elsevier Inc. This is an open access article under the CC BY-NC-ND license (<http://creativecommons.org/licenses/by-nc-nd/4.0/>).

abilities have larger posterior hippocampi than controls and bus drivers (Maguire et al., 2006). In addition to these experience-based morphological changes, *in-vivo* dynamics of microstructural integrity of the hippocampus have been demonstrated in association with sex-hormones, at much shorter time scales (Barth et al., 2016).

These structural changes in the hippocampus arise from variation at its local microstructural organizations. Nevertheless, considering the tight integration of hippocampus within the large scale brain networks and its high degree of structural, as well as functional, connectivity (Maller et al., 2019) with other brain regions, the observed morphological plastic changes could also be accounted by system-level interactions of the hippocampus with distinct brain regions.

As far, two organizational patterns have been proposed in the hippocampus. The first one is based on the long history of cytoarchitectonic mappings, evidencing reliable boundaries based on microscopic features, such as somatic size, shape and size (Andersen et al., 2007; Duvernoy, 2005), subdividing the hippocampus into different subfields. The hippocampal subfields spatially span along the proximal-distal axis, which is represented along the medio-lateral and the ventro-dorsal axes, in the *rolled-in*, volumetric representations (Fig. 1-A). In parallel, *in-vivo* examinations using electrophysiological recordings and task activations, as well as studies assessing connectivity patterns of the hippocampus, have suggested an organization along the anterior-posterior axis (Colombo et al., 1998; Przeździk et al., 2019; Strange et al., 2014).

In the recent years, many studies of the hippocampus have begun to focus more on this later organizational dimension. Multiple lines of evidence in animals and humans support the existence of such organizational pattern and its relevance for behavioral functions. In particular, it has been shown that the hippocampal projections to cortical and subcortical structures follow a graded pattern of connections changing gradually along its longitudinal axis (Strange et al., 2014). Also, gene expression studies have demonstrated a molecular gradient along the longitudinal axis, which is linked to distinct functional networks in the brain, each showing preferential vulnerability to different neurodegenerative conditions (Vogel et al., 2019). Interestingly, association with behavioral functions in the hippocampus have also shown a gradual change along the longitudinal axis (Plachti et al., 2018). According to these accumulating evidence, unlike the cytoarchitectonic organizational pattern, which is mainly related to local microscopic tissue properties, the longitudinal organizational pattern is driven by cortical and sub-cortical interactions of the hippocampus, demonstrating its tight integration within the large scale functional systems, enabling the hippocampus to sub-serve broad behavioral functions.

Data-driven approaches to parcellate the hippocampus based on its

connectivity profiles with the rest of the brain have demonstrated a differentiation in the connectivity patterns along the longitudinal axis, subdividing the head and tail of the hippocampus from more intermediate sections. In addition, the intermediate clusters are also separated into medial and lateral clusters (Plachti et al., 2018) (Fig. 1-B). Strikingly, the existence of such medial-lateral clusters in addition to the general pattern along the anterior-posterior axis of the hippocampus might be indicative of multiple superimposed organizational forces coming from innate microstructural characteristics (such as cytoarchitectonic and myelin features), as well as interaction with other brain regions. Such an interplay between long-range connectivity and local microstructural properties were demonstrated recently by Vos de Wael et al., identifying two main axes of functional connectivity transition within each of the hippocampal cytoarchitectonically-defined subfields. In particular, while the first axis demonstrated a gradual anterior to posterior transition of functional connectivity patterns with the rest of the brain, the second axis followed closely the distribution of myelin markers in most subfields. These results demonstrate the existence of overlapping functional organizational patterns, within each hippocampal subfield, presumably shaped by both, long-range connections as well as, the underlying microstructural properties.

Research on the dynamic properties of hippocampal structure and its morphological alterations in association with learning, aging, neurodegenerative diseases and its vulnerability to factors such as stress and hormonal alterations has a longer history than MRI-based functional evidence of a longitudinal gradient. However, as far, an integrative view on the existence and interplay between different organizational forces, shaping hippocampal structure and its morphological dynamic properties, is crucially lacking. Characterizing the major dimensions shaping the structural aspects of the hippocampus can open new perspectives to better understand the multifaceted role of the hippocampus in the complexity of the human cognitive systems, hippocampus' plasticity, as well as population's patterns of interindividual variability and, vulnerability to neurodegenerative diseases.

To identify and disentangle the major organizational modes of the hippocampal macrostructure, in the current study, we leveraged high-resolution multi-modal neuroimaging from the openly accessible HCP dataset. We examined hippocampal voxels with regards to their structural co-plasticity with the rest of the brain. We hence characterized the main dimensions of variability across hippocampal voxels with regard to similarity of their whole-brain structural covariance patterns. The thereby derived estimates of co-plasticity are called structural covariance (SC) and reflect the degree of co-variability in the structural properties of each hippocampal voxel with all other gray matter voxels, across a large group of individuals.

Previous studies have revealed the existence of multiple highly reproducible co-plastic networks consisting of distinct regions across the brain within cohorts of healthy individuals. Regions belonging to the same co-plastic network are suggested to demonstrate similar vulnerability to disease processes. Accordingly, pathologic conditions such as different types of neurodegenerative diseases, primarily affect regions that belong to the same co-plastic network (Evans, 2013; Seeley et al., 2009; Zhou et al., 2012). By definition, structural covariance is based on the similarity of the macrostructural variations (Mechelli et al. 2005; Alexander-Bloch et al. 2013) and thus is primarily influenced by factors influencing underlying structure, such as expression of common genetic cues during early development of the cortex (Raznahan et al., 2011) and direct structural connectivity through monosynaptic connection (Yee et al., 2018). Nevertheless, within healthy individuals, the co-plastic patterns also resemble functional networks derived from resting-state functional connectivity (RSFC) analysis, suggesting that the structural covariance also arises due to network mediated plasticity – as a result of plasticity-related changes at the synaptic and cellular levels (Evans, 2013). RSFC reflects the intrinsic patterns of signal co-fluctuations between two distinct regions and hence presumably functional interaction between regions. The structural properties of the regions that

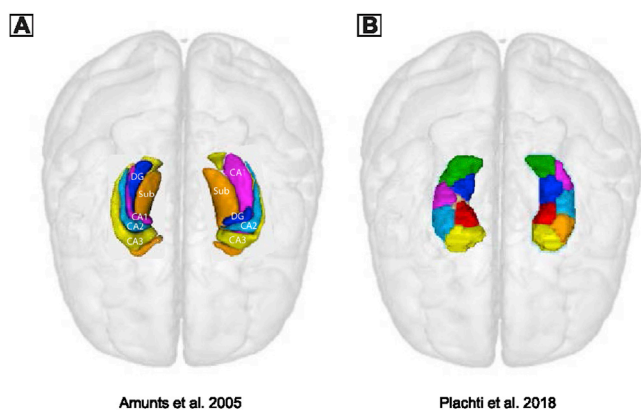


**Fig. 1.** Map of hippocampal cytoarchitectonic differentiation (Amunts et al., 2005) (A). Clustering of hippocampus from (Plachti et al., 2018), based on its pattern of resting-state functional connectivity, showing differentiation along the longitudinal axis but also a medial and lateral differentiation within the intermediate clusters (B). CA: cornu-ammonis; DG: dentate gyrus; Sub: subiculum.

demonstrate such functional coupling, co-vary to a high degree together as well (Alexander-Bloch et al., 2013a), hence conceptually linking RFSC and structural covariance networks (Kotkowski et al. 2018). In sum, structural covariance is assumed to reflect common influences of certain factors on microstructure, be it synaptogenesis based on functional synchronous firing, connectivity as direct monosynaptic connection, gene expression in synapses development, or similarities in the local micro-architectonic properties. In the current study, we use the information from this multi-facet covariance pattern to disentangle major dimensions of variability of the hippocampal co-plasticity.

In the first step, across a group of young participants from the HCP cohort, we identified the patterns of structural covariance of each voxel within the hippocampus and all none-hippocampal gray matter voxels. The similarity of the structural covariance patterns of every pairs of hippocampal voxels were then summarized in an affinity matrix. This latter was further decomposed into its major components using a diffusion map embedding approach (a non-linear manifold learning technique (Margulies et al., 2016)). In brief, the algorithm estimates a low-dimensional embedding from a high-dimensional similarity matrix. Within each new dimension, the voxels with more similar pattern of structural covariance are closer together and the voxels at the opposite ends of the gradient have the most different structural covariance patterns. Compared to other nonlinear manifold learning techniques, the algorithm is relatively robust to noise and computationally inexpensive (Tenenbaum et al., 2000).

Importantly, we assessed the replicability of these structural gradient patterns in an independent dataset. To further interpret these organizational axes, we assessed spatial similarity of major dimensions of structural covariance with variations in local microstructural properties, approximating myelin destitution, as well as cytoarchitectonic distinctions across the hippocampus. Furthermore, to investigate the relationship between structural and functional organization patterns within the hippocampus, major modes of variations in the functional connections and co-activation patterns of the hippocampal voxels with the rest of the brain were derived using the same decomposition approach.

Our analysis revealed a principal gradient of structural covariance that followed the hippocampal longitudinal axis and corresponded to the main dimension of functional connectivity variation in the hippocampus. The second gradient, demonstrated a dorsal-medial organization, and was moderately associated with the spatial distribution of proxy measures of myelin in hippocampus. It also showed a moderate link with cytoarchitectonic classifications, suggesting a partial link between this second dimension of structural covariance and the hippocampal innate microstructural properties.

## 2. Methods

### 2.1. Participants

The participants of the main analysis were selected from the publicly available data from the Human Connectome Project (HCP; <http://www.humanconnectome.org>), consisting of young healthy adults. HCP comprises data from 1113 individuals (656 females), with mean age of 28.8 years (standard deviation (SD) = 3.7, range = 22–37). The full set of inclusion and exclusion criteria are described elsewhere (Glasser et al., 2013; Van Essen et al., 2013). Here we selected a subset of *unrelated* individuals from this cohort, consisting of 377 individuals (age:  $28 \pm 3.6$ , 192 female), with good quality structural and four available resting-state functional scans.

For replication sample, healthy adult participants from the enhanced NKI (eNKI) Rockland cohort (Nooner et al., 2012) were selected. We focused only on participants for which good quality T1-weighted scans were available. Exclusion criteria consisted of alcohol or substance dependence or abuse (current or past), psychiatric illnesses (eg. Schizophrenia) and current depression (major or bipolar). Furthermore, we excluded participants with bad quality of structural scans after

pre-processing, resulting in a total sample of 468 healthy participants (age:  $48 \pm 19$ , 315 female).

### 2.2. MRI acquisition and preprocessing

#### 2.2.1. Structural MRI

MRI data of the main sample (HCP) were acquired on the HCP's custom 3T Siemens Skyra. Two T1w images with identical parameters were acquired using a 3D-MPRAGE sequence (0.7 mm isotropic voxels, TR = 2400 ms, TE = 2.14 ms, flip angle =  $8^\circ$ ; iPAT = 2). Two T2w images were acquired with identical geometry (TR = 3200 ms, TE = 565 ms, variable flip angle; iPAT = 2).

The imaging data of the eNKI cohort were all acquired using a single scanner (Siemens Magnetom TrioTim, 3.0 T). T1-weighted images were obtained using a MPRAGE sequence (1 mm isotropic voxels, TR = 1900 ms; TE = 2.52 ms).

#### 2.2.2. Rs-fMRI

Within the HCP cohort, four rs-fMRI scans were acquired using multi-band accelerated 2D-BOLD echo-planar imaging (2 mm isotropic voxels, matrix =  $104 \times 90$ , 72 sagittal slices; TR = 720 ms, TE = 33 ms, flip angle =  $52^\circ$ ; mb factor = 8; 1200 vol/scan). Participants were instructed to keep their eyes open, look at fixation cross, and not fall asleep.

### 2.3. Image processing

#### 2.3.1. Structural MRI

Both datasets were preprocessed using the CAT12 toolbox (Gaser and Dahnke, 2016). Briefly, each participant's T1-weighted scan was corrected for bias-field inhomogeneities, then segmented into gray matter (GM), white matter (WM), and cerebrospinal fluid (CSF) (Ashburner and Friston, 2005). The segmentation process was further extended for accounting for partial volume effects (Tohka et al., 2004) by applying adaptive maximum a posteriori estimations (Rajapakse et al., 1997). The gray matter segments were then spatially normalized into standard (MNI) space using Dartel algorithm (Ashburner, 2007) and further modulated. The modulation was performed by scaling the normalized gray matter segments for the non-linear transformations (only) applied at the normalization step. While this procedure ignores the volume changes due to affine transformation, it allows preserving information about individual differences in *local* gray matter volume. In other words, it re-introduces individual differences in local gray matter volume removed in the process of inter-subject registration and normalization. Finally, the modulated gray matter images were resampled to a voxel resolution of 2 mm isotropic.

#### 2.3.2. T1-weighted over T2-weighted ratio

For each individual, the bias-corrected T2-weighted images were co-registered to the individual's T1-weighted scan using a rigid-body transformation model. The ratio of the two scans (T1w/T2w) is then generated for each individual and warped to the standard (MNI) space using deformation fields, calculated from application of Dartel algorithm on the participant's T1-weighted data. The warped T1w/T2w-ratio maps were also resampled to a voxel resolution of 2 mm isotropic.

#### 2.3.3. Rs-fMRI

Pre-processed resting-state timeseries were downloaded from the ConnectomeDB (<https://db.humanconnectome.org>). Briefly, for each participant, the timeseries were corrected for gradient nonlinearity, and head motion was corrected using a rigid body transformation. The geometric distortions were corrected using the R-L/L-R blipped scan pairs. Distortion corrected images were warped to T1w space using a combination of rigid body and boundary-based registrations (Greve and Fischl, 2009). These transformations were concatenated with the transformation from native T1w to MNI152, to warp functional images to MNI152. After removing the bias field, brain extraction and normalization of whole

brain intensity was done. A high-pass filter ( $>2000$ s full-width-half-maximum) corrected the time series for scanner drifts. Further noise was removed using the ICA-FIX procedure (Salimi-Khorshidi et al., 2014). Finally, the preprocessed resting-state scans, with a voxel resolution of 2 mm, were smoothed with an isotropic gaussian kernel of 5 mm (full-width-half-maximum).

#### 2.4. Hippocampal volume of interest (VOI) and gray matter target

We defined our VOI as a consortium of the cytoarchitectonic maps, available in the SPM Anatomy Toolbox 2.0 (Eickhoff et al. 2005), and the macro anatomically-defined Harvard-Oxford Structural Probability Atlas ([http://neuro.imm.dtu.dk/wiki/Harvard-Oxford\\_Atlas](http://neuro.imm.dtu.dk/wiki/Harvard-Oxford_Atlas)) (Desikan et al. 2006). The hippocampal formation included the following subfields: CA1–3, dentate gyrus, and subiculum. In addition, by thresholding average of the modulated gray matter images from the HCP cohort to values above 0.2, a whole brain gray matter mask was generated. The aforementioned hippocampal VOIs are further restricted by this gray matter mask. The total number of voxels in a  $2\text{ mm} \times 2\text{ mm} \times 2\text{ mm}$  space in the right hippocampus was 771 and that of the left hippocampus was 756 voxels.

Furthermore, as target mask for covariance (structural/functional) analyses, the hippocampal VOIs were dilated by 8 mm (isotropic) and the resulting regions (both the left and right dilated-hippocampal VOIs) were excluded from the above-mentioned thresholded whole-brain gray matter mask. This procedure aims to diminish the possibility of mixing of the signal from the hippocampal voxels in the target, which may otherwise occur, for example as a result of smoothing. The remaining gray matter voxels (including cerebral and cerebellar, as well as subcortical gray matter) were used as target mask.

#### 2.5. Hippocampal connectivity analysis

##### 2.5.1. Structural covariance

Within each cohort, structural covariance (SC) was measured by computing the Pearson's correlation coefficient between gray matter volume values of the hippocampus' VOI voxels (seed voxels per hemisphere) and all other brain gray matter voxels across the whole sample. This procedure yielded one seed-by-target structural covariance matrix, at the group level, for each of the hippocampal VOIs (i.e. one pre hemisphere).

To reduce noise and increase between participant overlap of gray matter structures, in particular in the highly folded cortical regions, the target voxels were selected from modulated gray matter images that were additionally smoothed with an isotropic gaussian kernel of 8 mm (full-width-half-maximum). The seed voxels (hippocampal VOI) were, however, selected from resampled, modulated gray matter segments with no further smoothing.

##### 2.5.2. Resting-state functional connectivity analysis

For every participant, resting-state functional connectivity (RSFC) was assessed for every session, by calculating the Pearson's correlation between time courses of seed voxels and target voxels, both extracted from the preprocessed, smoothed resting-state scans of each session. Then the FC matrices were averaged across the four sessions, within each participant and were standardized using the Fisher's Z-transformation. By averaging the resulting z-scored, averaged FC-matrices across all participants, one seed-by-target overall mean FC-matrix was created, for each of the hippocampal VOIs (i.e. one pre hemisphere).

##### 2.5.3. Task-based co-activation analysis

As an additional measure of functional interaction, or connectivity, we characterized task-based **co-activation profiles**, between hippocampal seed voxels and the rest of the brain (cfs (Plachti et al., 2018)). These **co-activation profiles** were investigated using seed-based activation likelihood estimation meta-analysis of functional neuroimaging

data stored in the BrainMap database (Laird et al. 2011) (<http://www.brainmap.org>). To account for spatial uncertainty, the nearest 100 experiments reporting activation within each seed voxel or in its immediate vicinity were considered. The brain-wide **co-activation pattern** for each seed voxel was then computed by a quantitative meta-analysis, using the revised ALE algorithm (Eickhoff et al. 2012), over the retrieved experiments. **This analysis resulted in one seed-by-target co-activation matrix, for each of the hippocampal VOIs (i.e. one per hemisphere).**

#### 2.6. Gradient mapping

We utilized diffusion embedding, an unsupervised learning algorithm, to identify principal modes of spatial variations in covariance pattern across the entire of hippocampal voxels, per hemisphere. Briefly, for each modality, the overall (per hemisphere) hippocampal connectivity (covariance) matrix, was proportionally thresholded at 90% per row, retaining only the top 10% correlations between each hippocampal voxel and the target gray matter voxels. This sparse thresholded, asymmetric covariance matrix was then transformed into a normalized angle matrix (based on affinity matrix created based on cosine similarities, resulting in a non-negative and symmetric similarity matrix. Then diffusion map embedding, a one-parameter ( $\alpha$ ) family of graph Laplacians that integrates local information into a global description, was applied on this normalized angle matrix, to obtain a low-dimensional representation of the covariance matrix, explaining the variance in descending order (each of  $1 \times \text{\#VOI voxels}$ ). See Fig. 2 for schematic representation of these steps. In line with previous neuroimaging studies, e.g. (Bayrak et al., 2019; Margulies et al., 2016; Vos de Wael et al., 2018), we used an  $\alpha$  of 0.5, resulting in diffusion maps that retain the global relations between data points in the embedded space and are more robust to noise in the covariance matrix.

Voxels along each gradient map are assigned unitless embedding values. Along each gradient (columns of the embedding matrix on the right, in Fig. 2), voxels that share similar covariance pattern have similar embedding values. For further details see (Margulies et al., 2016; Vos de Wael et al., 2018).

#### 2.7. Statistical analysis

##### 2.7.1. Major gradients of structural covariance matrix and their between-sample replicability

In order to assess between-sample replicability of major modes of variation in the structural covariance across the hippocampal voxels, the structural covariance maps were generated, as mentioned earlier, for the HCP and eNKI datasets **separately**, and the diffusion map embedding algorithm was then applied for each VOI, **on each sample's affinity matrix**. The resulting gradient maps were ordered according to the explained variance, **within each dataset**. We then assessed similarity of the distribution of the gradients across the datasets, **by calculating spatial Spearman's rank correlations between pairs of gradients derived from the two datasets**. As the sign of the gradients are arbitrary, for all correlations, we report only the absolute coefficients.

##### 2.7.2. Exploring the relation between hippocampal structural gradients and functional gradients

To explore the association between the major modes of structural covariance variation and hippocampal local microstructural properties, the T1wT2w-ratio maps were masked using the VOI mask of each hippocampus and the distribution of the values within each hemisphere were correlated with the distribution of the values for each gradient separately, using Spearman's rank correlations.

To characterize the influence of cytoarchitectonic differentiations on the patterns of structural covariance gradients, we used the Jülich cytoarchitectonic atlas (<https://juba.in.fz-juelich.de/apps/cytoviewer/cytoviewer-main.php#>), released as part of FSL-package and compared the distribution of the gradient values between its main subdivisions



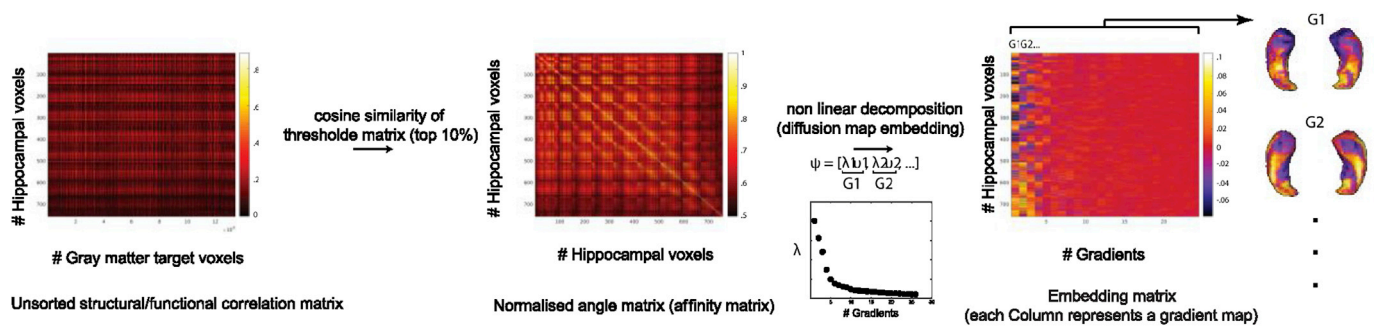


Fig. 2. Schematic description of the analysis steps.  $\lambda$  : eigen values of the transition matrix.  $G$  : gradient.

using Wilcoxon-Mann-Whitney-tests (significance was set at  $p$ -value  $< 0.0002$ , correcting for multiple comparison for the four gradients and three subdivisions using Bonferroni correction). For this, we masked the hippocampus, within each hemisphere, using the cornu-ammonis (CA), dentate gyrus and subiculum masks. **Distribution of the gradient values of the voxels belonging to each of the masked subregions are then compared with each other to investigate the possible impact of cytoarchitectonic differentiations on the generation of the observed pattern of structural covariance of the hippocampus.**

### 3. Results

#### 3.1. Gradients of hippocampal structural covariance and their between sample replicability

The spatial distributions of the first four gradients of the structural connectivity within the HCP cohort are presented in Fig. 3 and Supplementary Figure 1. In total, these four principal gradients explained more than 55% of variance of the data in each hemisphere (left: 55%; right: 58%) and corresponded to the clearest elbow in the scree plot (Fig. 3).

The first gradient of structural covariance ( $G1_{SC}$ ), which explained more than 20% of the variance (left: 20%; right: 24%) showed an

anterior-posterior organization along the longitudinal axis of the hippocampus. The second gradient ( $G2_{SC}$ ) depicted a general dorsal-ventral and partly medio-lateral gradient pattern, explaining 16% of variance, in each hemisphere (Fig. 3). Finally, the third and fourth gradients of structural covariance ( $G3_{SC}$  and  $G4_{SC}$ ), each explaining  $\sim 10\%$  of variance ( $G3_{SC}$ : left: 12%; right: 10%;  $G4_{SC}$ : left: 7%; right: 8%) showed a mixed pattern of differentiation along the longitudinal direction but also in the orthogonal directions, in the medio-lateral and dorsal-ventral directions, respectively (Supplementary Figure 1).

To confirm that these organizational patterns of the structural covariance were not sample specific, we ran the same approach on 468 participants of the eNKI sample, which covers a larger age-range than the HCP participants. Fig. 4 demonstrates the spatial correlation of the first four gradients of the two datasets. Accordingly, in both hemispheres the first gradient of the eNKI cohort also demonstrated an anterior-posterior organization and had a high spatial correspondence ( $\rho > 0.7$ ), showing similar organization of the voxels in the first principal gradient along the longitudinal axis of the hippocampus, as compared to the HCP sample. In this dataset, the principal gradient explained 16% and 18% of variance in the left and right hemisphere, respectively.

Further examinations of the similarity of the organization of the voxels in the subsequent gradients in the eNKI dataset suggested high

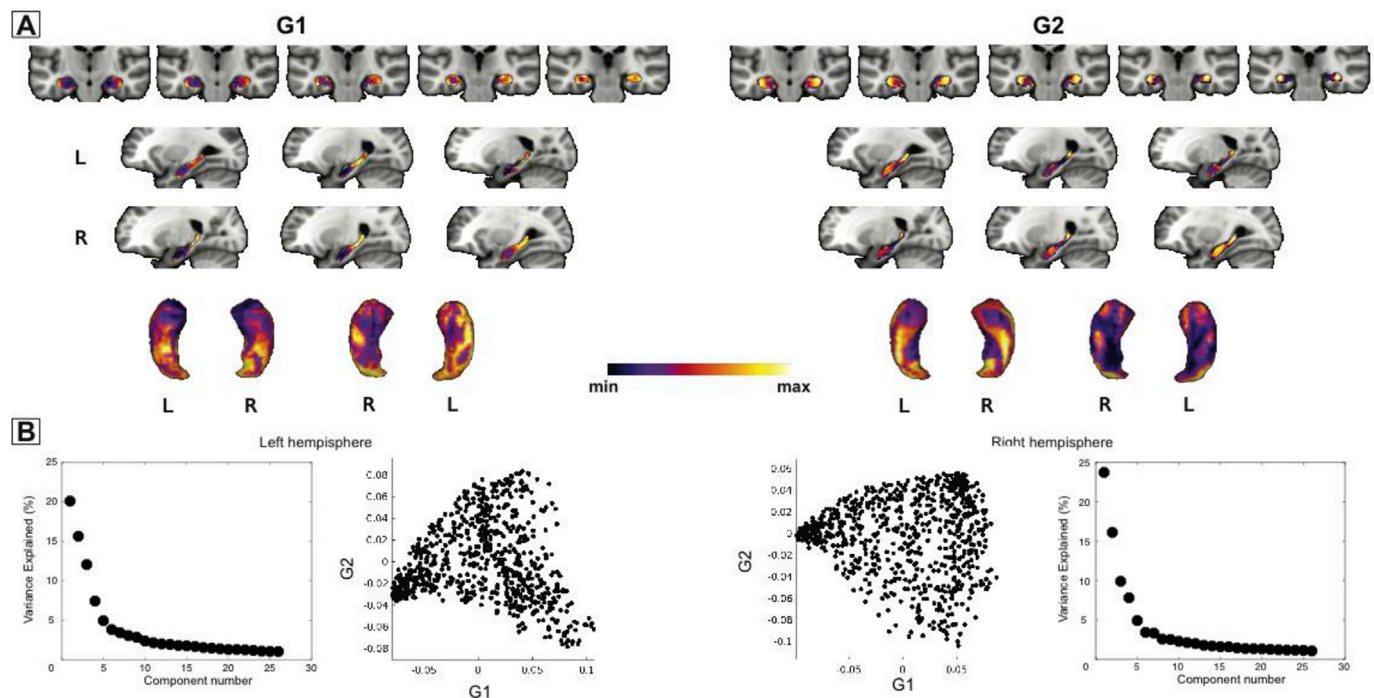
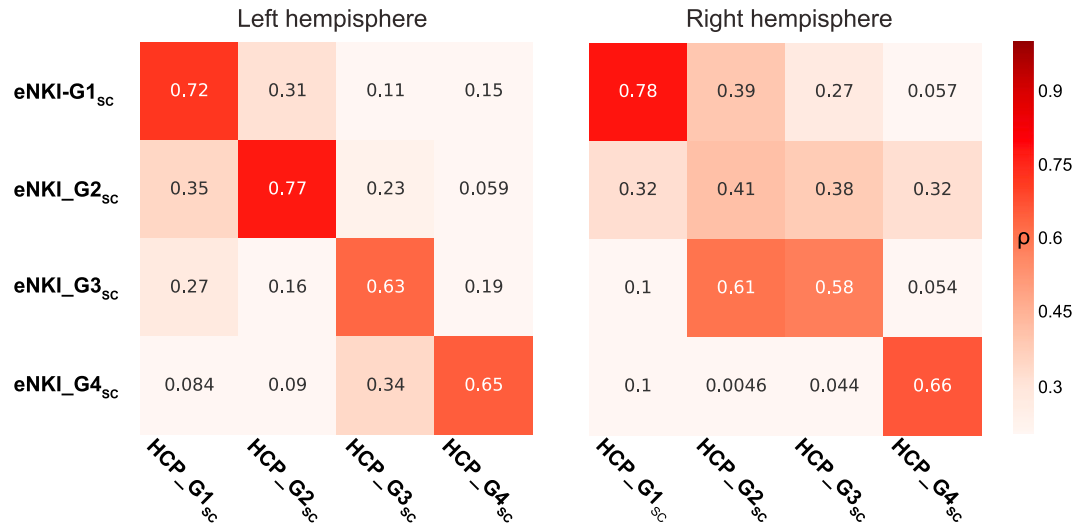


Fig. 3. A: Spatial maps of the first two principle gradients of the structural covariance of the hippocampus. For better visualization, colormaps show ranked gradients. Opposite ends of the colormap, depict voxels with the most distinct pattern of structural covariance with the rest of the brain. B: Variance explained by the diffusion-embedding components (left and right hemisphere). For each hemisphere the scatter plot of the first two connectivity embedding gradients are also shown.



**Fig. 4.** Absolute spearman's rank correlation coefficient ( $\rho$ ) between corresponding diffusion-embedding components from structural covariance maps derived within the HCP (columns) and eNKI (rows) sample. G: gradient; SC: structural covariance.

correlation ( $\rho > 0.63$ ) with the same ordering of the HCP dataset in the left hemisphere. In the right hemisphere, while the forth gradient of the eNKI sample correlated mostly with the forth gradient (G4<sub>sc</sub>) of the HCP sample, the second and third gradients showed a more mixed spatial patterns, correlating with both G2<sub>sc</sub> and G3<sub>sc</sub> in the HCP cohort ( $\rho > 0.38$ ). In addition, in both, the left and right hemisphere, the first and second gradients from the eNKI cohort also correlated moderately ( $\rho > 0.3$ ) with G2<sub>sc</sub> from the HCP cohort. Similarly to what we observed in the HCP dataset, within the eNKI sample, the first four gradients, captured more than 50% of the variance (left hemisphere: 15%, 14%, 7%; right hemisphere: 17%, 12%, 7%, demonstrating the variance explained by the second, third and fourth components, respectively).

So, in sum, in both datasets, more than 50% of the SC pattern can be summarized into four gradients whose spatial patterns are replicable across both datasets. In the right hemisphere, the second and third gradients did not show a clear one to one mapping between cohorts suggesting that these two gradients could differently vary across different datasets, but in the left hemisphere, a relative one to one correspondence could be evidenced.

### 3.2. Highly similar functional and structural main organizational patterns in the hippocampus

To investigate the similarity of the organizational patterns of the hippocampal voxels based on structural covariance with the organizational patterns of the hippocampal voxels based on functional connectivity, we utilized two independent measures of functional connectivity: RSFC and meta-analytic **task-based co-activation**. As Fig. 5 shows, the first gradient of the structural covariance (G1<sub>sc</sub>) from the HCP cohort correlated strongly with the principal gradient of both functional modalities (G1<sub>RSFC</sub>  $\rho = 0.7$  and  $0.79$ ; Co-activation  $\rho = 0.58$  and  $0.73$ , in the left and right hemisphere, respectively). This main functional gradient, just like the G1<sub>sc</sub>, exhibited a dominant anterior-posterior organization (see Supplementary Figure 2) and explained  $\sim 30\%$  of variance in either hemisphere in both functional modalities. In general, these results demonstrate the existence of a general smooth transition along the longitudinal hippocampal axis, that represent the major mode of variation in hippocampal structural and functional covariance/connectivity patterns.

The first and third gradients of **task-based co-activations** further showed moderate association with the third gradient of structural covariance (G3<sub>sc</sub>) ( $\rho \sim 0.4$ ), in both hemispheres, suggesting a partial

pattern of medial-lateral gradient in the major modes of variability of **task-based co-activations**. The other gradients of either of the functional data did not show consistently strong (i.e. similarly strong in both hemispheres) pattern of spatial association with the remaining structural gradients.

### 3.3. Relationships of hippocampal structural gradients with estimates of microstructure and cytoarchitectonic organization

The spatial maps of the distribution patterns of T1wT2w-ratio (used to estimate myelin) in the bilateral hippocampus showed moderate association ( $\rho > 0.34$ ) with the second gradient of structural covariance (G2<sub>sc</sub>), in the HCP cohort (see Supplementary Figure 3 for spatial maps of the distribution patterns of T1wT2w-ratio). In addition, within the left hemisphere, T1wT2w-ratio also spatially correlated with G1<sub>sc</sub> ( $\rho = 0.36$ ).

Further subdividing the hippocampus into broad cytoarchitectonic territories, using the subregions cornu-ammonis (CA) and subiculum showed a tendency towards a consistent (i.e. in both hemispheres) pattern of higher gradient values in the CA field, compared to the subiculum region, in the second gradient of the structural covariance (G2<sub>sc</sub>) (p-value of the Mann-Whitney U tests in both hemispheres  $< 10^{-5}$  (Fig. 6). Of note, to avoid biased conclusions, due to relatively smaller size of the dentate gyrus compared to CA field ( $\sim 11$  times) and subiculum ( $\sim 6$  times), Fig. 6 only presents the results of comparison between CA and subiculum subfields. Comparison across all the three subregions are shown in the supplementary Figure 4.

These results suggest that, unlike the principal anterior-posterior structural covariance gradient that could be more associated with system-level interactions of the hippocampus with the rest of the brain, the second major mode of variation in the structural covariance of the hippocampus is more tightly linked to its local microstructural properties.

## 4. Discussion

In the current work, we investigated hippocampal structural organization, in terms of its co-plasticity patterns with the rest of the brain. We found that the main principal dimension of the structural covariance in the hippocampus depicts an anterior-posterior gradient hence suggesting that the predominant pattern of co-plasticity with the rest of the brain follows a smooth change across the hippocampal longitudinal axis. We

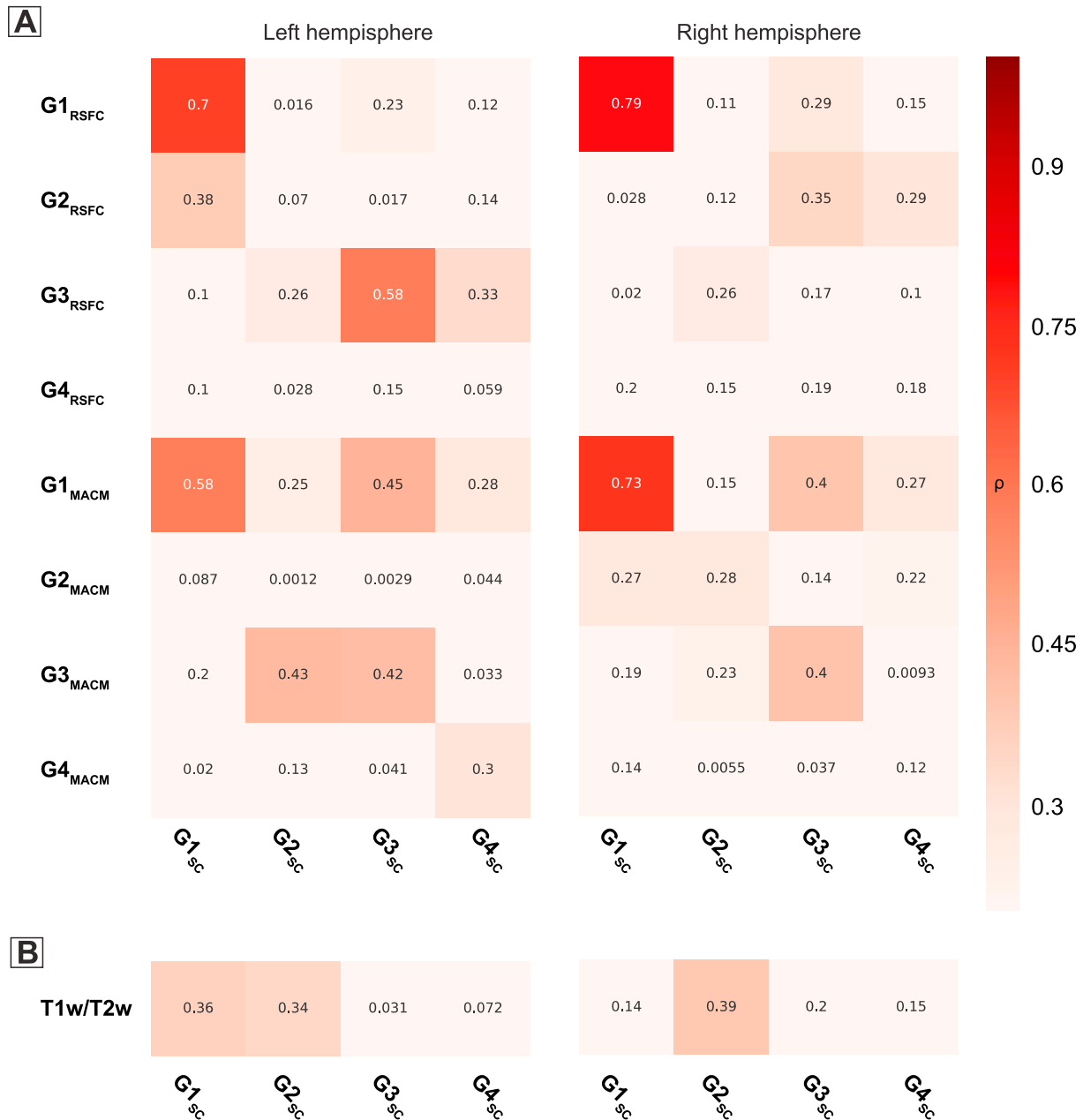


**Fig. 5.** A: Absolute spearman's rank correlation coefficient ( $\rho$ ) between corresponding diffusion-embedding components from the functional connectivity measures (rows) and structural covariance maps (columns) derived within the HCP cohort. B: Association between spatial distribution of T1w/T2w-ratio values and the major four gradients of structural covariance in the HCP cohort, defined using spearman's rank correlation. Darker colors represent stronger associations. . G: gradient; SC: structural covariance; RSFC: resting state functional connectivity; MACM: meta-analytic connectivity modelling; T1w: T1-weighted scan; T2w: T2-weighted scan.

demonstrated the high replicability of this organizational pattern in an independent dataset, consisting of participants with a broader age range hence confirming the generalizability of this main axis of co-plasticity variation across datasets. A similar anterior-posterior organization has been very recently shown as a major dimension of functional connectivity change within the hippocampus (Przeździk et al., 2019; Vos de Wael et al., 2018). Here we replicated this finding using both, resting-state and task-based functional connectivity/co-activation information and highlighted that a large proportion (~50%) of variance in the principal structural gradient of the hippocampus could be explained by this main pattern of functional configuration.

The examination of the subsequent structural gradients suggested a very limited similarity of the second dimension of structural variations and functional organization dimensions. Rather, the second major mode of variation in the structural covariance of the hippocampus

demonstrated a predominantly dorsal-ventral organization and was bilaterally moderately associated with the spatial distribution of myelin markers in the hippocampus, suggesting a partial link between this organizational pattern and hippocampal innate microstructural properties. Below we discuss the integration of these findings with very recent literature and emerging views in brain mapping, as well as the potential limitations of our study.

#### 4.1. Disentangling overlapping modes of structural covariance change for a unifying model of hippocampal organization

Understanding the organizational patterns of the brain that subserve information processing in health and explain behavioral phenotypes in pathology are crucial open questions in systems and clinical neuroscience. The study of brain organization is often complicated by evidence of

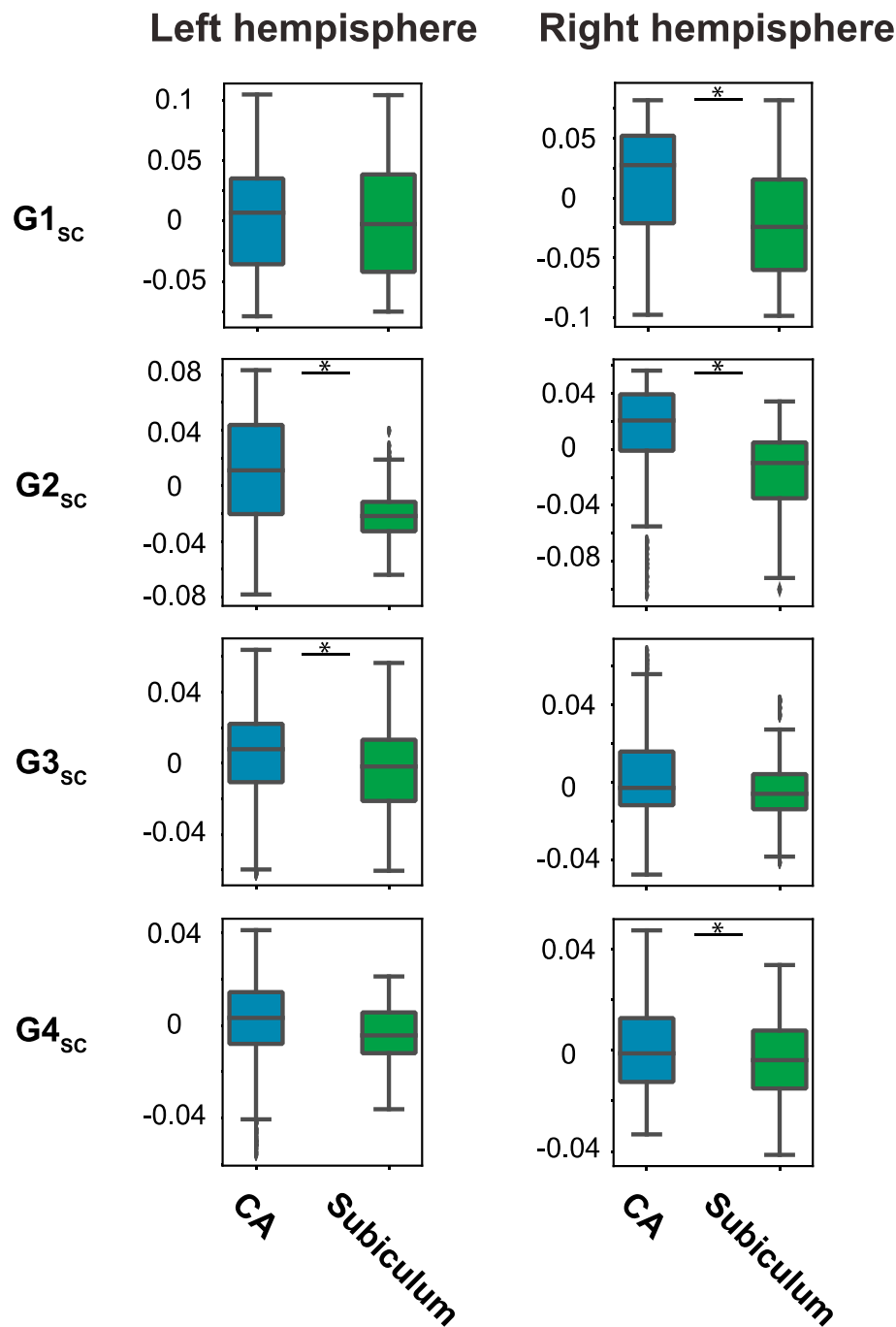


**Fig. 6.** Boxplots showing distribution of the gradient values within the CA and subiculum subfields, across the major four gradients of structural covariance in each hemisphere; Significant difference is shown using \* and shows  $p < 0.002$  of the Wilcoxon-Mann-Whitney-test. SC: structural covariance; CA: cornu-ammonis; G: gradient.

multiple axes of organization that are found with respect to different neurobiological properties (Eickhoff et al., 2018). For example, traditional mapping of the brain organization used local properties such as myelo- and cytoarchitectonic information to characterize brain regions and their relative organization (Hopf and Vitzthum, 1957; von Economo and Koskinas, 1925). Recent advances in *in-vivo* neuroimaging has expanded the scope of mapping brain organizational principles to the study of network-level interactions and characterizing overlapping axes of information processing and have hence revealed multiple organization dimensions (see (Haak et al., 2018) and (Genon et al., 2018, 2017) for recent examples, depicting such multiple dimensions of organization in the visual and premotor cortices, respectively).

The co-existence of these overlapping (i.e. spatially co-existing) and yet, distinct (i.e. from their properties) organizational principles and the interplay between them may give rise to the functional/behavioral specifications of brain regions and determine distinct neurocognitive patterns in pathologic conditions.

In particular, considering the hippocampal complex role in multiple different behavioral domains, its distinct cytoarchitectonic properties, its importance as a hub node in the human connectome and its involvement in multiple disorders, understanding its multiple organizational principles, may provide novel insights towards a unifying model of the hippocampus and its variabilities in health and disease. In the current study we examined the change in the structural covariance patterns of the



hippocampal voxels with the rest of the brain, to disentangle the different dimensions of its structural organization.

Structural covariance, defined as coordinated change in the local morphological properties between distinct pairs of brain regions across a population, reflects long-range co-plasticity. Shared genetic influences, direct structural connections (Yee et al., 2018), similarity of micro-structural properties and coordinated growth (Alexander-Bloch et al., 2013b), shared vulnerability towards toxic agents but also co-activation and co-firing of neurons, all may shape the pattern of structural co-plasticity of a given brain region. From this standpoint, the study of structural covariance may provide unique information about the interaction between these local and global factors and their relative representations on hippocampal neuroimaging-derived macrostructural properties.

#### 4.2. The main dimension of structural covariance of the hippocampus map onto the anterior-posterior functional differentiation

The major principal gradient of the structural covariance, running in the anterior/posterior direction, explained more than 20% of variance in the whole data and demonstrated a smooth transition pattern of structural co-plasticity across the longitudinal axis of the hippocampus. Our investigation of the replicability of the principal dimensions of hippocampal structural covariance in an independent dataset confirmed the sample-independence of this core finding. In other words, our results demonstrated the existence of a generalizable strong organization principle, governing hippocampal co-plastic patterns across its major longitudinal axis, among healthy individuals.

Multiple lines of evidence pointed out the pattern of differentiation of hippocampal properties along its longitudinal axis. In particular, a recent study have determined a gradual pattern of gene expression along the hippocampal longitudinal axis (Vogel et al., 2019). Similarly, associations with behavioral function, defined from task-activation meta-analytic analysis, indicated an emotion-cognition gradient along the anterior-posterior axis of the hippocampus, e.g. (Moser and Moser, 1998). However, the strongest support for the existence of an organizational principle along the hippocampal long-axis comes from its patterns of connectivity with the rest of the brain. Indeed, anatomical projections and electrophysiological recordings in rodent have demonstrated a gradual variation in the connectivity patterns of the hippocampus along the longitudinal axis (Strange et al., 2014). Similarly, in humans, using resting-state functional connectivity analysis, it has been shown that the large-scale functional interaction properties follow a dominant gradual change across hippocampal longitudinal axis (Vos de Wael et al., 2018). In the same line, our findings of strong spatial correlations between the major gradient of the structural covariance and functional connectivity analyses, suggest that the major organizational structural principle within the hippocampus may be enforced through long-range functional synchronous firing and **task co-activation**.

These findings can be related to the evidence of differential involvement of the anterior and posterior hippocampus in different neurodegenerative diseases (LaJoie et al., 2014b; Lee et al., 2017). In particular, our findings can be related to the differential impact of different pathologies, for example Amyloid/Tau pathology versus TDP-43-pathies (Lladó et al., 2018), in atrophy along the hippocampal longitudinal axis and hence provide a system-level explanation for the mechanisms underlying these pathologic changes and the related behavioral phenotypes. For instance, while many studies have shown local atrophy within the hippocampus, in both Alzheimer's disease and semantic dementia, it is known that the behavioral phenotype differ to a relatively large extent between these two diseases, with episodic memory being mainly impaired in the former. (LaJoie et al., 2014a). Interpreted the differential behavioral outcomes linked to hippocampal changes in terms of the variabilities of global functional interactions of the hippocampus within distinct large-scale networks in the two diseases. Similar complementary interpretations were found when considering the local

hypermetabolism along the hippocampal longitudinal axis, that were linked to differential network-level interactions and hence were associated with different behavioral symptoms among patients with depression compared to schizophrenic patients (Small et al., 2011). These findings provide evidence that specific aspects of local structural variations in the hippocampus are explained through the study of hippocampal global interactions, opening doors towards the identification of mechanistic biomarkers differentiating patients' specific profile across the disease spectrum.

#### 4.3. Linking additional dimensions of hippocampal structural covariance to local structural properties

The local microstructural properties of the hippocampus, unlike the distribution of its functional interaction and behavioral associations, do not predominantly differentiate along the anterior/posterior axis (DeKraker et al., 2019). Instead, the distinctions within the hippocampus based on the histological findings have been mainly defined across the dorsal-ventral and medial-lateral direction (proximal-distal axis), showing mainly that the structural properties of the hippocampus differentiate roughly orthogonal to its longitudinal axis and allowing the definition of subfields.

As a major principal organizational rule of the hippocampus, we expected to find an impact of the variations in these local structural properties in the structural covariance gradients. Accordingly, we found a moderate association between the spatial distributions of T1wT2w ratio, a proxy marker of myelin density, and the second gradient from the structural covariance data, in both hemispheres. These moderate associations suggests a link between the second dimension of macrostructural organization and the hippocampal internal circuitry (Augustinack et al., 2010; Zeineh et al., 2017). Linking the crude cytoarchitectonic differentiations to gradients from the structural covariance also showed a tendency in the CA subfield and subiculum to load on opposite ends of the second gradient. Since proximity in the gradient space reflects the similarity of the patterns of structural covariance, these findings suggest that, in the second main mode of structural covariance, the voxels in the CA show in general a distinct pattern of covariance with other gray matter voxels than the patterns shown by the voxels within the Subiculum. **Although caution should be taken when interpreting these findings, due to the wide range of the values within each subfield,** the trend in difference between subfields is congruent with our recent clustering of hippocampus' voxels based on their structural covariance pattern in healthy adults (Plachti et al., 2018). Indeed, applying a clustering algorithm to cluster hippocampus voxels based on the similarity of their brain co-plasticity pattern reveal a differentiation within the hippocampus body and tail that resembles the CA vs. Subiculum differentiation. Thus, altogether, the results of our previous clustering study together with the results of the current study suggest the partial influence of underlying microstructural properties in the pattern of structural covariance of hippocampus' voxels.

The distribution of *in-vivo* markers of myelin are shown to demonstrate differences across hippocampal subfields, with the highest levels of myelin concentrations being found in the subiculum (DeKraker et al., 2018; Patel et al., 2019; Vos de Wael et al., 2018). The elevated myelin estimate within this subfield could be assumed to partly result from the perforant path, passing through the subiculum, conceptually linking myelin distribution to subfield boundaries (DeKraker et al., 2018).

Finally, further dimensions of structural covariance, despite their general high degree of cross-sample replicability, did not show stable association with the functional gradients. Furthermore, their associations with the distribution of T1wT2w-ratio in the whole hippocampus and the atlas-defined cytoarchitectonic differentiations were also negligible. Altogether, these lack of associations suggest that these second-order dimensions cannot be characterized by our current estimates of myelin and a crude cytoarchitectonic differentiation. **This could be related to the limited neurobiological validity of our estimates and/or to**

**associations with unexplored neurobiological features. The possible methodological limitations of our study are further discussed below.**

#### 4.4. Challenges in linking patterns of structural covariance to local structural properties

An important aspect of the structural covariance analysis is the group-wise nature of the analysis, in which the covariance pattern of each voxel is defined based on correlation of morphological properties with the rest of the brain across a group of participants. Therefore, it requires the same definition of voxels across all participants of the cohort. Accordingly, to achieve such cross-individual correspondence, the structural images are preprocessed and registered to a common template, where gray matter volumes are defined within the same voxel on the template image for each individual. The procedure of registering single participant's structural data to the template involves multiple linear and non-linear deformations and thus can result in considerable inaccuracies, in particular when considering distinctions between small sub-regions within the hippocampus. Such inaccuracies should be considered in the identification of the subfields and their deformation from histological scans to the MNI template space. The cumulative impact of these deformation and registration inaccuracies, can in turn disguise the impact of the underlying cytoarchitectonic properties in the computation of separate dimensions of large-scale structural covariance patterns. To overcome this limitation, some studies used a subject-wise estimate of the subfields, derived from automatic classifications of the structural (T1w and T2w MRI) scans that are already registered to the template space, e.g. (Vos de Wael et al., 2018). However, due to possible inter-individual differences in the shape and size of the subfields, these algorithms are followed by further reparameterizations to improve correspondence of voxels across subjects, which can result in similar inaccuracies, particularly for structural covariance analysis, where the correlations are assessed as a result of group-level variations.

Additionally, linking the microstructural properties to the major modes of structural covariance variation is limited by the restricted neurobiological validity of the T1wT2w-ratio as an *in-vivo* marker of myelin (Arshad et al., 2017; Hagiwara et al., 2018; Uddin et al., 2018). The use of more direct and quantitative *in-vivo* correlates of myelin (Weiskopf et al., 2013) and even combination of multiple modalities (such as additional use of markers of white matter integrity and myelin density from diffusion MRI scans (Patel et al., 2019)) may provide more detailed information about how the underlying micro-structural variabilities are represented and possibly shape the macro-structural co-plasticity and co-atrophy patterns of the hippocampal voxels. These scientific developments could in turn help to explain the specific aspects of local vulnerability of the hippocampus in pathologic conditions.

#### 4.5. Conclusions and future perspectives

The current study aimed to disentangle the major modes of variation in the similarity of hippocampal voxels in terms of their co-plastic properties. Here we demonstrated that using a data-driven decomposition approach, the major modes of variation of the structural covariance patterns could be identified reliably across independent datasets with different age ranges. This replicability allows us to assume that the major dimensions shown in this study reflect generalizable patterns and are caused by general principles governing hippocampus' organization.

In this regard we showed that the principal component of the structural covariance followed the hippocampal longitudinal axis, depicting a smooth gradient running from the head to the tail and hence suggesting a smooth transition in the covariance patterns along this axis. The spatial pattern depicted by this gradient correlated highly with the major gradient of the functional connectivity analysis, suggesting an influence of global connectivity and co-firing in the realization of the main mode of variation in the structural covariance patterns in the hippocampus. In

contrast, the second gradient of structural covariance ran in the orthogonal direction mainly along the dorsal-ventral side and was moderately associated with hippocampal microstructural properties and cytoarchitectonic differentiation.

Considering the multi-faceted nature of the structural covariance information, further research incorporating more local and global complementary information, including gene expression patterns (Vogel et al., 2019), global white-matter connectivity patterns (Maller et al., 2019) and more quantitative measures of local micro-structural properties (Menon et al., 2019; Weiskopf et al., 2013) can help to further understand the underlying organizational forces generating different co-plastic modes in health and to characterize the vulnerability patterns between and within different pathologic conditions.

#### Ethics statement

This study used publicly released Human Connectome Project (HCP) dataset. Reanalysis of the data from the HCP cohort have been permitted through the local ethics committee of the university of Düsseldorf.

#### Declaration of competing interest

The authors declare no competing interests.

#### Acknowledgments

This work was supported by the Deutsche Forschungsgemeinschaft (DFG, GE 2835/1-1, EI 816/4-1), the Helmholtz Portfolio Theme 'Supercomputing and Modelling for the Human Brain' and the EEuropean Union's Horizon 2020 Research and Innovation Programme under Grant Agreement No. 785907 (HBP SGA2). Data were provided by the Human Connectome Project, WU-Minn Consortium (Principal Investigators: David Van Essen and Kamil Ugurbil; 1U54MH091657) funded by the 16 NIH Institutes and Centers that support the NIH Blueprint for Neuroscience Research; and by the McDonnell Center for Systems Neuroscience at Washington University.

#### Appendix A. Supplementary data

Supplementary data to this article can be found online at <https://doi.org/10.1016/j.neuroimage.2020.116972>.

#### References

- Alexander-Bloch, A., Giedd, J.N., Bullmore, E., 2013a. Imaging structural co-variance between human brain regions. *Nat. Rev. Neurosci.* 14, 322–336. <https://doi.org/10.1038/nrn3465>.
- Alexander-Bloch, A., Raznahan, A., Bullmore, E., Giedd, J., 2013b. The convergence of maturational change and structural covariance in human cortical networks. *J. Neurosci.* 33, 2889–2899. <https://doi.org/10.1523/JNEUROSCI.3554-12.2013>.
- Allen, G., Barnard, H., McColl, R., Hester, A.L., Fields, J.A., Weiner, M.F., Ringe, W.K., Lipton, A.M., Brooker, M., McDonald, E., Rubin, C.D., Cullum, C.M., 2007. Reduced hippocampal functional connectivity in alzheimer disease. *Arch. Neurol.* 64, 1482. <https://doi.org/10.1001/archneur.64.10.1482>.
- Amunts, K., Kedo, O., Kindler, M., Pieperhoff, P., Mohlberg, H., Shah, N.J., Habel, U., Schneider, F., Zilles, K., 2005. Cytoarchitectonic mapping of the human amygdala, hippocampal region and entorhinal cortex: intersubject variability and probability maps. *Anat. Embryol.* 210, 343–352. <https://doi.org/10.1007/s00429-005-0025-5>.
- Andersen, P., Morris, R., Amaral, D., Bliss, T., O'Keefe, J., 2007. *The hippocampus Book*. Oxford University Press. <https://doi.org/10.1002/hipo.20355>.
- Arshad, M., Stanley, J.A., Raz, N., 2017. Test-retest reliability and concurrent validity of in vivo myelin content indices: myelin water fraction and calibrated T1w/T2w image ratio. *Hum. Brain Mapp.* 38, 1780–1790. <https://doi.org/10.1002/hbm.23481>.
- Ashburner, J., 2007. A fast diffeomorphic image registration algorithm. *Neuroimage* 38, 95–113. <https://doi.org/10.1016/j.neuroimage.2007.07.007>.
- Ashburner, J., Friston, K.J., 2005. Unified segmentation. *Neuroimage* 26, 839–851. <https://doi.org/10.1016/j.neuroimage.2005.02.018>.
- Augustinack, J.C., Helmer, K., Huber, K.E., Kakunoori, S., Zölle, L., Fischl, B., 2010. Direct visualization of the perforant pathway in the human brain with ex vivo diffusion tensor imaging. *Front. Hum. Neurosci.* 4, 42. <https://doi.org/10.3389/fnhum.2010.00042>.

- Barth, C., Steele, C.J., Mueller, K., Rekkas, V.P., Arélin, K., Pampel, A., Burmann, I., Kratzsch, J., Villringer, A., Sacher, J., 2016. In-vivo dynamics of the human Hippocampus across the menstrual cycle. *Sci. Rep.* 6, 32833. <https://doi.org/10.1038/srep32833>.
- Bayrak, Ş., Khalil, A.A., Villringer, K., Fiebach, J.B., Villringer, A., Margulies, D.S., Oviada-Caro, S., 2019. The impact of ischemic stroke on connectivity gradients. *NeuroImage Clin* 24. <https://doi.org/10.1016/j.nicl.2019.101947>.
- Bonnici, H.M., Chadwick, M.J., Maguire, E.A., 2013. Representations of recent and remote autobiographical memories in hippocampal subfields. *Hippocampus* 23, 849–854. <https://doi.org/10.1002/hipo.22155>.
- Cha, J., Greenberg, T., Song, I., Blair Simpson, H., Posner, J., Mujica-Parodi, L.R., 2016. Abnormal hippocampal structure and function in clinical anxiety and comorbid depression. *Hippocampus* 26, 545–553. <https://doi.org/10.1002/hipo.22566>.
- Chersi, F., Burgess, N., 2015. The cognitive architecture of spatial navigation: hippocampal and striatal contributions. *Neuron* 88, 64–77. <https://doi.org/10.1016/j.neuron.2015.09.021>.
- Clawson, W., Vicente, A.F., Ferraris, M., Bernard, C., Battaglia, D., Quilichini, P.P., 2019. Computing hubs in the hippocampus and cortex. *Sci. Adv.* 5, eaax4843 <https://doi.org/10.1126/sciadv.aax4843>.
- Colombo, M., Fernandez, T., Nakamura, K., Gross, C.G., 1998. Functional differentiation along the anterior-posterior axis of the Hippocampus in monkeys. *J. Neurophysiol.* 80, 1002–1005. <https://doi.org/10.1152/jn.1998.80.2.1002>.
- Dalton, M.A., McCormick, C., Maguire, E.A., 2019. Differences in functional connectivity along the anterior-posterior axis of human hippocampal subfields. *Neuroimage* 192, 38–51. <https://doi.org/10.1016/j.neuroimage.2019.02.066>.
- DeKraker, J., Ferko, K.M., Lau, J.C., Köhler, S., Khan, A.R., 2018. Unfolding the hippocampus: an intrinsic coordinate system for subfield segmentations and quantitative mapping. *Neuroimage* 167, 408–418. <https://doi.org/10.1016/j.neuroimage.2017.11.054>.
- DeKraker, J., Lau, J.C., Ferko, K.M., Khan, A.R., Köhler, S., 2019. Hippocampal subfields revealed through unfolding and unsupervised clustering of laminar and morphological features in 3D BigBrain. *Neuroimage* 116328. <https://doi.org/10.1016/j.neuroimage.2019.116328>.
- Duvernoy, H.M., 2005. *The Human Hippocampus: Functional Anatomy, Vascularization, and Serial Sections with MRI*. Springer.
- Eichenbaum, H., 2004. Hippocampus: cognitive processes and neural representations that underlie declarative memory. *Neuron* 44, 109–120. <https://doi.org/10.1016/j.neuron.2004.08.028>.
- Eickhoff, S.B., Yeo, B.T.T., Genon, S., 2018. Imaging-based parcellations of the human brain. *Nat. Rev. Neurosci.* <https://doi.org/10.1038/s41583-018-0071-7>.
- Evans, A.C., 2013. Networks of anatomical covariance. *Neuroimage* 80, 489–504. <https://doi.org/10.1016/j.neuroimage.2013.05.054>.
- Fateh, A.A., Long, Z., Duan, X., Cui, Q., Pang, Y., Farooq, M.U., Nan, X., Chen, Y., Sheng, W., Tang, Q., Chen, H., 2019. Hippocampal functional connectivity-based discrimination between bipolar and major depressive disorders. *Psychiatry Res. Neuroimaging*, 284, 53–60. <https://doi.org/10.1016/j.pscychresns.2019.01.004>.
- Gaser, C., Dahnke, R., 2016. Cat - a computational anatomy toolbox for the analysis of structural MRI data. In: *HBM Conf.* 2016, 32, p. 7743.
- Genon, S., Li, H., Fan, L., Müller, V.I., Cieslik, E.C., Hoffstaedter, F., Reid, A.T., Langner, R., Grefkes, C., Fox, P.T., Moebus, S., Caspers, S., Amunts, K., Jiang, T., Eickhoff, S.B., 2017. The right dorsal premotor mosaic: organization, functions, and connectivity. *Cerebr. Cortex* 27, 2095–2110. <https://doi.org/10.1093/cercor/bhw065>.
- Genon, S., Reid, A., Li, H., Fan, L., Müller, V.I., Cieslik, E.C., Hoffstaedter, F., Langner, R., Grefkes, C., Laird, A.R., Fox, P.T., Jiang, T., Amunts, K., Eickhoff, S.B., 2018. The heterogeneity of the left dorsal premotor cortex evidenced by multimodal connectivity-based parcellation and functional characterization. *Neuroimage* 170, 400–411. <https://doi.org/10.1016/j.neuroimage.2017.02.034>.
- Glasser, M.F., Sotiropoulos, S.N., Wilson, J.A., Coalson, T.S., Fischl, B., Andersson, J.L., Xu, J., Jbabdi, S., Webster, M., Polimeni, J.R., Van Essen, D.C., Jenkinson, M., WU-Minn HCP Consortium, for the W.-M.H., 2013. The minimal preprocessing pipelines for the Human Connectome Project. *Neuroimage* 80, 105–124. <https://doi.org/10.1016/j.neuroimage.2013.04.127>.
- Greve, D.N., Fischl, B., 2009. Accurate and robust brain image alignment using boundary-based registration. *Neuroimage* 48, 63–72. <https://doi.org/10.1016/j.neuroimage.2009.06.060>.
- Haak, K.V., Marquand, A.F., Beckmann, C.F., 2018. Connectopic mapping with resting-state fMRI. *Neuroimage*. <https://doi.org/10.1016/j.neuroimage.2017.06.075>.
- Hagiwara, A., Hori, M., Kamagata, K., Wamties, M., Matsuyoshi, D., Nakazawa, M., Ueda, R., Andica, C., Koshino, S., Maekawa, T., Irie, R., Takamura, T., Kumamaru, K.K., Abe, O., Aoki, S., 2018. Myelin measurement: comparison between simultaneous tissue relaxometry, magnetization transfer saturation index, and T1w/T2w ratio methods. *Sci. Rep.* 8 <https://doi.org/10.1038/s41598-018-28852-6>.
- Halliday, G., 2017. Pathology and hippocampal atrophy in Alzheimer's disease. *Lancet Neurol.* 16, 862–864. [https://doi.org/10.1016/S1474-4422\(17\)30343-5](https://doi.org/10.1016/S1474-4422(17)30343-5).
- Hopf, A., Vitzthum, H.G., 1957. Über die Verteilung myeloarchitektonischer Merkmale in der Scheitellappenrinne beim Menschen. *J. Hirnforsch.* 3, 79–104.
- Kemmotsu, N., Kucukboyaci, N.E., Cheng, C.E., Girard, H.M., Tecoma, E.S., Iragui, V.J., McDonald, C.R., 2013. Alterations in functional connectivity between the hippocampus and prefrontal cortex as a correlate of depressive symptoms in temporal lobe epilepsy. *Epilepsy Behav.* 29, 552–559. <https://doi.org/10.1016/j.yebeh.2013.09.039>.
- LaJoie, R., Landeau, B., Perrotin, A., Bejanin, A., Egret, S., Pélerin, A., Mézenge, F., Belliard, S., deLaSayette, V., Eustache, F., Desgranges, B., Chételat, G., 2014a. Intrinsic connectivity identifies the hippocampus as a main crossroad between alzheimer's and semantic dementia-targeted networks. *Neuron* 81, 1417–1428. <https://doi.org/10.1016/j.neuron.2014.01.026>.
- LaJoie, R., Landeau, B., Perrotin, A., Bejanin, A., Egret, S., Pélerin, A., Mézenge, F., Belliard, S., deLaSayette, V., Eustache, F., Desgranges, B., Chételat, G., 2014b. Intrinsic connectivity identifies the hippocampus as a main crossroad between alzheimer's and semantic dementia-targeted networks. *Neuron* 81, 1417–1428. <https://doi.org/10.1016/j.neuron.2014.01.026>.
- Lee, A.R., Kim, J.H., Cho, E., Kim, M., Park, M., 2017. Dorsal and ventral hippocampus differentiate in functional pathways and differentially associate with neurological disease-related genes during postnatal development. *Front. Mol. Neurosci.* 10, 331. <https://doi.org/10.3389/fnmol.2017.00331>.
- Lieberman, J.A., Girgis, R.R., Brucato, G., Moore, H., Provenzano, F., Kegeles, L., Javitt, D., Kantrowitz, J., Wall, M.M., Corcoran, C.M., Schobel, S.A., Small, S.A., 2018. Hippocampal dysfunction in the pathophysiology of schizophrenia: a selective review and hypothesis for early detection and intervention. *Mol. Psychiatr.* 23, 1764–1772. <https://doi.org/10.1038/mp.2017.249>.
- Lladó, A., Tort-Merino, A., Sánchez-Valle, R., Falgàs, N., Balasa, M., Bosch, B., Castellví, M., Olives, J., Antonell, A., Hornberger, M., 2018. The hippocampal longitudinal axis—relevance for underlying tau and TDP-43 pathology. *Neurobiol. Aging* 70, 1–9. <https://doi.org/10.1016/j.neurobiolaging.2018.05.035>.
- Maguire, E.A., Woollett, K., Spiers, H.J., 2006. London taxi drivers and bus drivers: a structural MRI and neuropsychological analysis. *Hippocampus* 16, 1091–1101. <https://doi.org/10.1002/hipo.20233>.
- Maller, J.J., Welton, T., Middione, M., Callaghan, F.M., Rosenfeld, J.V., Grieve, S.M., 2019. Revealing the hippocampal connectome through super-resolution 1150-direction diffusion MRI. *Sci. Rep.* 9, 2418. <https://doi.org/10.1038/s41598-018-37905-9>.
- Maren, S., Holt, W., 2000. The hippocampus and contextual memory retrieval in Pavlovian conditioning. *Behav. Brain Res.* 110, 97–108. [https://doi.org/10.1016/S0166-4328\(99\)00188-6](https://doi.org/10.1016/S0166-4328(99)00188-6).
- Margulies, D.S., Ghosh, S.S., Goulas, A., Falkiewicz, M., Huntenburg, J.M., Langs, G., Bezgin, G., Eickhoff, S.B., Castellanos, F.X., Petrides, M., Jefferies, E., Smallwood, J., 2016. Situating the default-mode network along a principal gradient of macroscale cortical organization. *Proc. Natl. Acad. Sci. United States Am.* 113, 12574–12579. <https://doi.org/10.1073/pnas.1608282113>.
- Menon, V., Guillermo, G., Pinski, M.A., Nguyen, V.-D., Li, J.-R., Cai, W., Wassermann, D., 2019. Quantitative modeling links in vivo microstructural and macrofunctional organization of human and macaque insular cortex, and predicts cognitive control abilities. *bioRxiv* 662601. <https://doi.org/10.1101/662601>.
- Mitra, A., Snyder, A.Z., Hacker, C.D., Pahwa, M., Tagliazucchi, E., Laufs, H., Leuthardt, E.C., Raichle, M.E., 2016. Human cortical-hippocampal dialogue in wake and slow-wave sleep. *Proc. Natl. Acad. Sci. U. S. A.* 113, E6868–E6876. <https://doi.org/10.1073/pnas.1607289113>.
- Moser, M.B., Moser, E.I., 1998. Functional differentiation in the hippocampus. *Hippocampus* 2–7. [https://doi.org/10.1002/\(SICI\)1098-1063\(1998\)8:6<608::AID-HIPO3>3.0.CO;2](https://doi.org/10.1002/(SICI)1098-1063(1998)8:6<608::AID-HIPO3>3.0.CO;2).
- Nooner, K.B., Colcombe, S.J., Tobe, R.H., Mennes, M., Benedict, M.M., Moreno, A.L., Panek, L.J., Brown, S., Zavitz Stephen, T.T., Li, Q., Sikka, S., Gutman, D., Bangaru, S., Schlachter, R.T., Anwar, S.M.K., Hinz, C.M., Kaplan, M.S., Rachlin, A.B., Adelsberg, S., Cheung, B., Khanuja, R., Yan, C., Courtney, C.C.C., King, M., Wood, D., Cox, C.L., Kelly, A.M.C., Petkova, E., Reiss, P.T., Duan, N., Thomsen, D., Biswal, B., Coffey, B., Hoptman, M.J., Javitt, D.C., Pomara, N., Sidtis, J.J., Koplewicz, H.S., Castellanos, F.X., Leventhal, B.L., Milham, M.P., 2012. The NKI-Rockland sample: a model for accelerating the pace of discovery science in psychiatry. *Front. Neurosci.* <https://doi.org/10.3389/fnins.2012.00152>.
- Patel, R., Steele, C.J., Chen, A., Patel, S., Devenyi, G.A., Germann, J., Tardif, C.L., Chakravarty, M.M., 2019. Investigating microstructural variation in the human hippocampus using non-negative matrix factorization. *Neuroimage* 116348. <https://doi.org/10.1016/j.neuroimage.2019.116348>.
- Plachti, A., Eickhoff, S.B., Hoffstaedter, F., Patil, K.R., Laird, A.R., Fox, P.T., Amunts, K., Genon, S., 2018. Multimodal parcellations and extensive behavioral profiling tackling the Hippocampus gradient. *Cerebr. Cortex* 1–18. <https://doi.org/10.1093/cercor/bhy336>.
- Przeździł, I., Faber, M., Fernández, G., Beckmann, C.F., Haak, K.V., 2019. The functional organisation of the hippocampus along its long axis is gradual and predicts recollection. *Cortex* 119, 324–335. <https://doi.org/10.1016/j.cortex.2019.04.015>.
- Rajapakse, J.C., Giedd, J.N., Rapoport, J.L., 1997. Statistical approach to segmentation of single-channel cerebral mr images. *IEEE Trans. Med. Imag.* 16, 176–186. <https://doi.org/10.1109/42.563663>.
- Raznahan, A., Lerch, J.P., Lee, N., Greenstein, D., Wallace, G.L., Stockman, M., Clasen, L., Shaw, P.W., Giedd, J.N., 2011. Patterns of coordinated anatomical change in human cortical development: a longitudinal neuroimaging study of maturational coupling. *Neuron* 72, 873–884. <https://doi.org/10.1016/j.neuron.2011.09.028>.
- Salimi-Khorshidi, G., Douaud, G., Beckmann, C.F., Glasser, M.F., Griffanti, L., Smith, S.M., 2014. Automatic denoising of functional MRI data: combining independent component analysis and hierarchical fusion of classifiers. *Neuroimage* 90, 449–468. <https://doi.org/10.1016/j.neuroimage.2013.11.046>.
- Seeley, W.W., Crawford, R.K., Zhou, J., Miller, M.P., Barnes, C.A., 2009. Neurodegenerative diseases target large-scale human brain networks. *Neuron* 62, 42–52. <https://doi.org/10.1016/j.neuron.2009.03.024>.
- Small, S.A., Schobel, S.A., Buxton, R.B., Witter, M.P., Barnes, C.A., 2011. A pathophysiological framework of hippocampal dysfunction in ageing and disease. *Nat. Rev. Neurosci.* 12, 585–601. <https://doi.org/10.1038/nrn3085>.
- Stella, F., Treves, A., 2011. Associative memory storage and retrieval: involvement of theta oscillations in hippocampal information processing. *Neural Plast.* 2011, 683961. <https://doi.org/10.1155/2011/683961>.

- Strange, B.A., Witter, M.P., Lein, E.S., Moser, E.I., 2014. Functional organization of the hippocampal longitudinal axis. *Nat. Rev. Neurosci.* 15, 655–669. <https://doi.org/10.1038/nrn3785>.
- Tenenbaum, J.B., de Silva, V., Langford, J.C., 2000. A global geometric framework for nonlinear dimensionality reduction. *Science* 290, 2319–2323. <https://doi.org/10.1126/science.290.5500.2319>.
- Tohka, J., Zijdenbos, A., Evans, A., 2004. Fast and robust parameter estimation for statistical partial volume models in brain MRI. *Neuroimage* 23, 84–97. <https://doi.org/10.1016/j.neuroimage.2004.05.007>.
- Uddin, M.N., Figley, T.D., Marrie, R.A., Figley, C.R., 2018. Can T1w/T2w ratio be used as a myelin-specific measure in subcortical structures? Comparisons between FSE-based T1w/T2w ratios, GRASE-based T1w/T2w ratios and multi-echo GRASE-based myelin water fractions. *NMR Biomed.* 31, e3868 <https://doi.org/10.1002/nbm.3868>.
- Van Essen, D.C., Smith, S.M., Barch, D.M., Behrens, T.E.J., Yacoub, E., Ugurbil, K., 2013. The Wu-minn human connectome Project: an overview. *Neuroimage* 80, 62–79. <https://doi.org/10.1016/j.neuroimage.2013.05.041>.
- Vogel, J.W., Joie, R. La, Grothe, M.J., Diaz-Papkovich, A., Doyle, A., Vachon-Preseu, E., Lepage, C., Wael, R.V. de, Iturria-Medina, Y., Bernhardt, B., Rabinovici, G.D., Evans, A.C., 2019. A Molecular Gradient along the Longitudinal axis of the Human Hippocampus Informs Large-Scale Behavioral Systems. <https://doi.org/10.1101/587071> bioRxiv 587071.
- von Economo, C., Koskinas, G., 1925. *Die Cytoarchitektonik der Hirnrinde des erwachsenen Menschen*. Julius Springer, Berlin.
- Vos de Wael, R., Larivière, S., Caldairou, B., Hong, S.-J., Margulies, D.S., Jefferies, E., Bernasconi, A., Smallwood, J., Bernasconi, N., Bernhardt, B.C., 2018. Anatomical and microstructural determinants of hippocampal subfield functional connectome embedding. *Proc. Natl. Acad. Sci. Unit. States Am.* 115, 10154–10159. <https://doi.org/10.1073/pnas.1803667115>.
- Ward, A.M., Schultz, A.P., Huijbers, W., Van Dijk, K.R.A., Hedden, T., Sperling, R.A., 2014. The parahippocampal gyrus links the default-mode cortical network with the medial temporal lobe memory system. *Hum. Brain Mapp.* 35, 1061–1073. <https://doi.org/10.1002/hbm.22234>.
- Weiskopf, N., Suckling, J., Williams, G., Correia, M., M. M., Inkster, B., Tait, R., Ooi, C., Bullmore, T., E. T., Lutti, A., 2013. Quantitative multi-parameter mapping of R1, PD\*, MT, and R2\* at 3T: a multi-center validation. *Front. Neurosci.* 7, 95. <https://doi.org/10.3389/fnins.2013.00095>.
- Yee, Y., Fernandes, D.J., French, L., Ellegood, J., Cahill, L.S., Vousden, D.A., Spencer Noakes, L., Scholz, J., van Eede, M.C., Nieman, B.J., Sled, J.G., Lerch, J.P., 2018. Structural covariance of brain region volumes is associated with both structural connectivity and transcriptomic similarity. *Neuroimage* 179, 357–372. <https://doi.org/10.1016/j.NEUROIMAGE.2018.05.028>.
- Zeineh, M.M., Palomero-Gallagher, N., Axer, M., Gräsel, D., Goubran, M., Wree, A., Woods, R., Amunts, K., Zilles, K., 2017. Direct visualization and mapping of the spatial course of fiber tracts at microscopic resolution in the human Hippocampus. *Cerebr. Cortex* 27, 1779–1794. <https://doi.org/10.1093/cercor/bhw010>.
- Zhou, J., Gennatas, E.D., Kramer, J.H., Miller, B.L., Seeley, W.W., 2012. Predicting regional neurodegeneration from the healthy brain functional connectome. *Neuron* 73, 1216–1227. <https://doi.org/10.1016/j.neuron.2012.03.004>.